Effects of Interface Formation Process on electronic properties of n-type $Ti_{0.3}Zn_{0.7}O_{1.3}$/ p-type Si stack structure

Kenta Ogawa[1,2*], Toyohiro Chikyow[2], Yuki Daimon[1,2], Atsushi Ogura[1,3] and Takahiro Nagata[2,1*]

[1]*Graduate School of Science and Technology, Meiji University, 1-1-1 Higashimita, Tama-ku, Kawasaki, Kanagawa 214-8571, Japan*

[2]*National Institute for Materials Science (NIMS), 1-1 Namiki, Tsukuba, Ibaraki 305-0044, Japan*

[3]*Meiji Renewable Energy Laboratory, Meiji University, 1-1-1 Higashimita, Tama-ku, Kawasaki, Kanagawa 214-8571, Japan*

E-mail: ce241031@meiji.ac.jp, NAGATA.Takahiro@nims.go.jp

The interfacial properties between the oxide-based channel materials and Si were investigated with a view to their application in tunnel field effect transistors. We focused on $Ti_xZn_{1-x}O_{1+x}$, a solid solution of TiO_2 and ZnO, as the channel material, expecting that the high oxygen bond dissociation energy (E_{bd}) of Ti would suppress oxygen vacancies and interfacial states with Si. From the exploration of solid solution compositions by combinatorial method, we confirmed that a composition of x = 0.3 satisfies all the conditions of amorphous structure, low resistance, and low surface roughness. In addition, to understand the interfacial reactions between elements with different E_{bd} and Si, the intermediate SiO_2 layers were investigated by electrical properties and photoelectron spectroscopy. It was found that the $Ti_{0.3}Zn_{0.7}O_{1.3}$ film with an initial TiO_2 layer in a TiO_2/ZnO multiple stacked structure rather than a single $Ti_{0.3}Zn_{0.7}O_{1.3}$ target synthesis has less degradation of electrical properties and interfacial defects.

1. Introduction

In recent years, the Internet of Things, artificial intelligence, automated driving technology, and so on, has led to a demand for higher performance semiconductor devices and increased supply. On the other hand, the increase in power consumption of complementary metal oxide semiconductor (CMOS) integrated circuits has become a major concern. To solve this concern, it is necessary to explore the new materials used the channel and/or source materials of next generation transistors. We focused on $Ti_xZn_{1-x}O_{1+x}$, a solid solution of TiO_2 and ZnO, as a channel material with assuming application to tunnel field effect transistors (tunnel FETs). ZnO has high mobility and has already been put to practical use in a wide range of applications, such as material for thin-film transistors.[1-6] However, when using ZnO as a channel material for transistors, the flatness of the interface may be a problem because it easily crystallizes regardless of lattice mismatch.[7,8] In addition, when forming a film on a Si wafer, there is a concern that a SiO_2 layer may be unintentionally formed at the interface.[8,9] On the other hand, TiO_2 is widely used as a catalyst material and is relatively inexpensive.[10] In addition, Ti has a high oxygen bond dissociation energy [E_{bd}, Ti: 666 kJ/mol, Zn: 250 kJ/mol].[11,12] Previous research has reported that the stability of oxygen vacancies has been improved in In-Ti-O, which is an In_2O_3 material doped with Ti, and it is expected to control oxygen vacancies in oxide materials and improving interface properties.[13] For these reasons, we focused on $Ti_xZn_{1-x}O_{1+x}$, a solid solution of TiO_2 and ZnO, and in this paper, we conducted an evaluation focusing on the interface properties.

We are considering tunnel FETs as one of the applications of $Ti_xZn_{1-x}O_{1+x}$. Tunnel FETs operate by applying a positive voltage to the gate and drain to overlap the density of states (DOS) of the conduction band in the channel region and the valence band in the source region, and flowing band to band tunneling current between the source and drain.[14,15,16,17] The current of a tunnel FETs is expected to increase rapidly as soon as the overlapping of DOS and this phenomenon is known as the energy filtering effect.[15] Based on the above operating principle, tunnel FETs are expected that achieving steep current changes due to gate voltage control, high on-currents, high on/off current ratios, and small SS values that exceed the limit of Si-CMOS without being restricted by the Boltzmann distribution, and are being studied as the most feasible device.[18,19,20,21] The advantages of using oxide semiconductors and Si as channel/source materials for tunnel FETs are that type II

heterojunctions can be easily formed and the characteristics can be controlled by solid solutions and composition changes. In particular, type II heterojunctions can lower the effective barrier height without decreasing the band gap of the base material, and therefore are expected to have a high current on/off ratio.[19,21] In addition to these advantages, the $Ti_xZn_{1-x}O_{1+x}$, investigated in this study, improve the flatness of the interface due to the effect of Ti, which is expected to improve the tunneling properties compared with previous studies.

In this paper, we first prepared compositionally graded $Ti_xZn_{1-x}O_{1+x}$ films using combinatorial synthesis[22,23] to investigate the solid solution compositions suitable for tunnel FET channels and report the correlation between the composition ratio and the physical properties. Based on the results of compositionally graded $Ti_xZn_{1-x}O_{1+x}$ films, three different film structures were prepared by fixing the Ti composition to understand the interfacial reactions of Si with Zn and Ti with different E_{bd}. It is thought that this has a different effect on the formation of SiO_2 at the interface and the electrical properties. To be specific, two types of thin films with a multilayer structure of approximately one lattice thickness were prepared, in which ZnO and TiO_2 were alternately stacked. ZnO and TiO_2 were deposited as the first layer on Si substrates, respectively. In addition, one type of single-structure thin film was prepared using a target material with a mixed composition, for a total of three types.

2. Experimental methods

The compositionally graded $Ti_xZn_{1-x}O_{1+x}$ film was deposited on a p-Si (100) substrate by the combinatorial pulse laser deposition (PLD) system. A schematic diagram of the sample is shown in Figure 1 (a). The substrate was cleaned with an organic solvent solution and deionized water, followed by cleaning with HF solution. A KrF excimer laser (wavelength: 248 nm) was used as the laser source for PLD, and the oxygen partial pressure as set to 1×10^{-4} Torr. Ceramic sintered TiO_2 and ZnO targets were used, and film formation was performed using a combinatorial method in the order of ZnO to TiO_2 deposition alternatively. The substrate temperature was set to 300 °C and the film thickness was set to 10 nm. For electrical measurements, top electrodes of 20 nm thick Ti/100 nm thick Pt were deposited by DC magnetron sputtering. The top electrodes with a diameter of 110 μm were

patterned along the composition gradient using a metal mask, and the back electrode was a uniform metal film formed over the entire back of the substrate. Previous study has also confirmed the SiO_2 layer at the ZnSnO/p-Si interface, and it has been reported that the interfacial states in this SiO_2 layer trap carriers, causing degradation of electrical properties.[9] Since forming gas annealing (FGA) using hydrogen gas is effective in reducing these interfacial states,[24,25] samples were annealed by rapid thermal annealing (Advance Riko, MILA-3000) at 400 °C for 30 min under a forming gas of 4% H_2: N_2. Crystallinity was evaluated by two-dimensional X-ray diffraction (2D-XRD; Bruker AXS, D8 Discover). Surface roughness was evaluated from the route mean square roughness (RMS) value by an atomic force microscope (AFM; Hitachi High-Technologies, AFM5000II) using 5 measurement points with a composition ratio x from 0.0 to 1.0 in increments of 0.25. Electrical characteristics were evaluated by current-voltage (I-V) measurements using a semiconductor parameter analyzer (Keysight Technologies, B1500A). To measure resistivity, the compositionally graded $Ti_xZn_{1-x}O_{1+x}$ film was deposited on a quartz substrate and their resistivity was measured. The chemical bonding states and band alignment at the interface were evaluated by X-ray photoelectron spectroscopy (XPS; Thermo Scientific, K-Alpha and Sigma Probe) using a monochromatic Al Kα-X-ray source with an energy of 1.49 keV and a diameter of 400 μm at 6 measurement points with a composition ratio x from 0.0 to 1.0 in increments of 0.2. The total energy resolution was 700 meV. The obtained XPS data were calibrated against the C 1s peak, and the core-level spectra were fitted using the Voigt function after removing the background by the Shirley function.[26] For the compositionally graded $Ti_xZn_{1-x}O_{1+x}$ film, the measurements were performed using 11 measurement points with a composition ratio x from 0.0 to 1.0 in 0.1 increments, except for the AFM measurements and XPS measurements.

To investigate the effects of the interface formation of $Ti_xZn_{1-x}O_{1+x}$ film and Si on the electrical properties, $Ti_xZn_{1-x}O_{1+x}$ films with x of 0.3 were deposited on the Si (100) substrate. In addition to the TiO_2 and ZnO targets, a $Ti_{0.3}Zn_{0.7}O_{1.3}$ sintered target was also used to fabricate three structures, as shown in Figure 1 (b), (c) and (d). The interfacial formation processes of $Ti_{0.3}Zn_{0.7}O_{1.3}$, TiO_2, and ZnO with the Si substrate are different, and are referred to as “Single layer”, “TiO_2 first”, and “ZnO first”, respectively. In addition,

TiO_2 first and ZnO first have a multilayer structure in which alternating layers of about 0.4 nm thick layers are stacked on top of each other to adjust the ratio of TiO_2: ZnO as 3:7. Note that the composition was tuned by the growth rate and number of layers, and that the initial reaction was different, although the mixed reaction is thought to be induced from the kinetic energy from heating and laser excitation during deposition rather than from the atomic-level stacking structure. The film thickness was set to 5 nm to make it easier to observe the tunnel current component and detect changes in the interface. Then, an Al electrode was fabricated by evaporation on the surface of the substrate, and Ti and Pt electrodes were fabricated by DC sputtering on the back. This is because the evaporation reduces damage to the substrate surface compared to DC sputtering, and Al provides better contact. The voltage sweep direction was set to - to +. Other deposition, annealing, and measurement conditions were set to the same as for the composition gradient film. For these samples, to clearly detect the Si substrate, we also employ another XPS with dual x-ray sources of Cr and Al (ULVAC-PHI, PHI Quantes). The Cr Kα-x-ray has an energy of 5.42 keV, and is able to detect deeper depth than that of the Al Kα-x-ray. The total energy resolutions of Al Kα- and Cr Kα-XPS were 750 and 1100 meV, respectively. The X-ray spot sizes were both 100 μm in diameter. To identify the interface structure, X-ray reflectivity measurement (XRR) was also performed by using the 2D-XRD system. XRR measurements using incident X-rays of 1 mm diameter provided average information over a 10 mm range of the same composition and thickness on the sample, and the structure of the entire sample was analyzed. The reflections were fitted by DIFFRAC.LEPTOS software (Bruker AXS) with the genetic algorithm optimization of fitting parameters.

3. Results and discussion

3-1 Explore for solid solution compositions with amorphous structure and flat surface

As shown in Figure 2, the XRD patterns of the $Ti_xZn_{1-x}O_{1+x}$ film with a composition of x = 0.1 or less shows reflection at 2θ values of 34.5°, corresponding to the (0002) reflection of ZnO with the hexagonal structure. Note that, the 2D-XRD image of Ti composition of x = 0 and 0.1 showed the (0002) reflection with a broad spot pattern, meaning the film has an oriented structure with <0001> direction, as shown in the inset of Fig. 2. In contrast, when

the Ti composition was x = 0.2 or more, it was amorphous, and crystallization was not confirmed even with TiO_2 composition. ZnO is easily crystallized even at room temperature, and it is possible to obtain an orientation film without being affected by the substrate.[7] In contrast, TiO_2 is easily affected by the substrate. The substrate lattice mismatches of Si (100) with TiO_2 (100) with the rutile structure or (110) with anatase structure are 15.5 and 30.4%, respectively. It is possible to crystallize it by optimizing conditions such as gas pressure[27] or the intermediate layer formation,[28,29] but we think that the current conditions were able to suppress the crystallization. AFM observations confirmed that crystallization also affects surface roughness, as shown in Figure 3. The ZnO composition has a small grain structure and high roughness, whereas the grain structure becomes unclear, and the roughness decreases as the Ti composition increases. In the amorphous region, the RMS value is 0.12 nm or less, and a flat film with a minimum RMS value of 0.08 nm was confirmed. From the perspective of film thickness uniformity, it appears that a high TiO_2 ratio is more superior than low ratio as a thin film structure, but as shown in Fig. 3, a change in resistance was confirmed. Low resistivity derived from ZnO at a composition of $x \leqq 0.3$ was confirmed. The resistivity increases and then decreases gradually at a composition of $x \geqq 0.4$. This is thought to be due to the promotion of oxidation caused by the increase in Ti and/or the possibility of the formation of micro crystals of TiO_2. These can lead to variations in the current conduction distance and electron trapping due to degradation of the interface quality, so it seems that a composition of $x \geqq 0.4$ cannot be applied to transistor channel. In the previous study, an unintentional interface SiO_x layer has been formed between the oxide semiconductor and Si.[19] In this study, as shown in Figure 4, it is confirmed from XPS that the formation of SiO_x and the ratio of the interface oxide layer to Si increases with the increase in the composition ratio of TiO_2. The ratio also increases with post-annealing. It was found that the increase in Ti increases the controllability of the resistivity of the oxide semiconductor and the interfacial oxidation. From these results, we concluded that a composition of x = 0.3, which satisfies all the conditions of being amorphous, having low resistance, and low RMS, is expected to have useful for transistor channel.

To further improve the electrical and physical properties, it is necessary to understand the effects of elements in the solid solution with different oxidation energies on the

formation of the interfacial SiO_2 layer. Based on the above results, the band alignment of $Ti_xZn_{1-x}O_{1+x}$ /Si has the type II structure, however the unintentionally formed SiO_2 layer is inserted at the interface (SI, Fig. S1). In the next chapter, we fixed the composition ratio at x = 0.3 and investigated into the effects of three types of interface formation processes on the electronic properties.

3-2 Effects of Interface Formation Process on electronic properties

Figure 5 shows I-V characteristics for Single layer, TiO_2 first, and ZnO first. All samples showed rectification characteristics, but their shapes and slopes were different. In the case of Single layer, the current characteristics became closer to ohmic characteristics due to the increase in leakage current. The rectification property derived from the pn junction was observed in the cases of TiO_2 first and ZnO first, and the current rise at forward bias was steeper in TiO_2 first. However, the voltage shift indicating the minimum current value was also larger in TiO_2 first. To compare and clarify the differences in these I-V characteristics, we simply analyzed the current mechanisms of (1) tunneling current and (2) Poole-Frenkel emission as the following relationships.[30] Here, the "tunneling current" means the tunneling current caused by electrons tunneling from $Ti_{0.3}Zn_{0.7}O_{1.3}$ layer to the p-Si layer through the unintentionally formed SiO_2 layer, and the "Poole-Frenkel emission" means the current conduction via defect states in the $Ti_{0.3}Zn_{0.7}O_{1.3}$ layer or SiO_2 layer. In addition, the effects of Al electrode on I-V characteristics can be concerned in this measurement. Discussions are provided in Supplemental Information Fig. S2.

$$I = V^2 \exp\left(-\frac{1}{V}\right) \qquad (1)$$

$$I = V \exp\left(\sqrt{V}\right) \qquad (2)$$

Figure 6 (a) and (b) show replotted I-V characteristics using the (1) tunneling current and (2) Poole-Frenkel emission relations, respectively. These plots indicate the existence of each current component (1) and (2) in the range where the plots become linear. The voltage range is (1) 0.3 V to 1.0 V and (2) 0.05 V to 1.0, respectively. According to the previous study, since the non-linear line shown in Fig. 6 (a) is the overlap of the multiple tunneling current components caused by variations in the tunnel distance due to poor film thickness uniformity and interface flatness, and may lead to the degradation of the I-V characteristics

and the SS value,[18] it was suggested that TiO_2 first, which has the best linearity, has effective tunneling characteristics. Also, since the overlap of Pool-Frenkel emissions shown in Fig. 6 (b) means an increase in electron traps and which leads to poor I-V characteristics, it was suggested that ZnO first, which has the best linearity, is thought to have the fewest interfacial defects. Also, the reason for the increase in the voltage shift indicating the minimum current value in TiO_2 first was suggested the result of electron traps by tale states or interfacial states.

For Single layer, both AFM and XPS imply the issue of uniformity. Figure 7 shows AFM images. TiO_2 and ZnO first samples show quite flat and uniform surface with the RMS values less than 0.02 nm. In contrast, Single layer includes some particles. Table 1 shows the full width at half maximum (FWHM) values and Ti composition ratio to Zn calculated from the Zn $2p_{3/2}$ and Ti $2p_{3/2}$ spectra, as shown in Figure 8 (a) and (b). The spectral shape of XPS is affected by the distribution of electron density derived from chemical bonding or by the shift of the Fermi level. In the case of Single layer, all the spectra are shifted towards the high binding energy side compared to the other two samples, indicating that the Fermi level has shifted towards the conduction band. Furthermore, an increase in the FWHM was also observed, which suggests an increase in the defect structure and electrons derived from Ti although no significant difference was observed in the FWHM of Zn $2p_{3/2}$ spectra of all samples. In response to this, the O 1s shows an increase in peaks corresponding to defects on the high binding energy side, as shown in Fig. 8 (c). Furthermore, in the area intensity ratio of Zn $2p_{3/2}$ to Ti $2p_{3/2}$, only Single layer showed a large value, and reproducibility was not confirmed for several film thicknesses, with a variation of more than ±10%. Variations on several measurement points of O 1s area intensity in Single layer are shown in Supplemental Information Fig. S3. These results indicate that there is a possibility of variations in Ti composition and TiO_x phase separation in the single layer, which leads to degradations of the tunneling characteristics and the non-uniform interface. To understand the $Ti_{0.3}Zn_{0.7}O_{1.3}$/Si interface, we use the Si 1s spectra obtained by the Cr Kα-XPS. Si 1s is not affected by orbital splitting like Si 2p. In the present material, Zn 3p is present around 90 eV in the vicinity of Si 2p, and its tail on the high binding energy side affect the Si 2p background (SI, Fig. S4). In addition, due to its high binding energy, it detects relatively deep regions, so in this sample, it mainly

detects regions around the interface. Figure 9 shows Si 1s spectra normalized to the peak top of the bonding states of Si at the energy of 1839.33 eV. In addition to Si, there are three bonding states corresponding to SiO_2 (1843.99 eV), suboxide (Si^{3+}, 1843.34 eV), and intermediate layers of Si-Ti-O_x and Si-Zn-O_x (Si^{2+},1842.52 eV). The thickness of the SiO_2 layer is the thickest in Single layer, and it was found that the SiO_2 layer is thicker in TiO_2 first than in ZnO first. On the other hand, it can be seen that the thickness of the intermediate layer is thicker in ZnO first. This result suggests that the high oxygen bond dissociation energy of Ti and the low oxide formation energy suppressed the oxygen vacancy at the interface, and the oxygen bonded with Si to form a more stable in TiO_2 first. In contrast, it may be formed an unstable and thinner SiO_2 layer due to non-uniform oxygen vacancy in ZnO first. These differences were not limited to the microscopic region of the XPS spot size, but were also observed in the macroscopic region, as shown by the results of the XRR measurements in Figure 10. Each sample showed different shapes of reflections. Fitting parameters indicated that ZnO first showed the thinnest thickness of SiO_2. The variety of density and roughness also suggests the defect density.

The interfacial reactions suggested by all the results in this chapter are summarized in Figure 11. Ti segregation causes film defects and forms the non-uniform interface in Single layer. This leads to variations in the tunneling distance and an increase in the leakage currents. The high oxygen bond dissociation energy of Ti suppresses oxygen vacancy and forms a uniform interface in TiO_2 first. However, the interfacial SiO_2 layer, which has tail states and interfacial states, may be an issue of tunneling current reduction. The formation of non-uniform oxygen vacancies causes variations in the tunneling distance in ZnO first. This leads to non-steep current increase. However, because the SiO_2 layer is thinner than TiO_2 first, it is thought that reducing the Pool-Frenkel emission due to the few interfacial states. From the above, it is suggested that TiO_2 first has the most effective tunneling properties.

4. Conclusions

We explored for solid solution compositions of $Ti_xZn_{1-x}O_{1+x}$ and investigated the effects of three types of interface formation processes on the electronic properties since the Si interface has a significant influence on the physical properties and the elements with

different divergence energies are mixed. From the results of exploring the suitable solid solution composition as the transistor channel by combinatorial method, a composition of x = 0.3 satisfies all the conditions of amorphousness, low resistivity and low RMS. To study of the interfacial reactions, three different interface formation processes were investigated: a stacked structure of ZnO and TiO_2, each of which is the first layer deposited on the Si substrate, and a single synthesis. It was found that TiO_2 first forms the most stable unintentionally interfacial SiO_2 layer and has the most effective tunneling properties. These results suggest that $Ti_xZn_{1-x}O_{1+x}$ can control the formation of the interfacial SiO_2 layer by optimizing the composition ratio and the interfacial formation process, and improve the electrical properties.

Acknowledgments

We are grateful to Ms. A. Ogawa and Ms. M. Watanabe for technical support with the fabrication and evaluation method, respectively. A part of this work was supported by "Advanced Research Infrastructure for Materials and Nanotechnology in Japan (ARIM)" of the Ministry of Education, Culture, Sports, Science and Technology (MEXT). Proposal Number JPMXP1223NM5168 and JPMXP1224NM5066.

References

[1] K. Nomura, H. Ohta, A. Takagi, T. Kamiya, M. Hirano and H. Hosono, *Nature*, **432**, p.488 (2004).

[2] K. Kurishima, T. Nabatame, M. Shimizu, S. Aikawa, K. Tsukagoshi, A. Ohi, T. Chikyo, and A. Ogura, ECS Trans., **61**, p.345–351 (2014).

[3] K. Kurishima, T. Nabatame, M. Shimizu, N. Mitoma, T. Kizu, S. Aikawa, K. Tsukagoshi, A. Ohi, T. Chikyow, and A. Ogura, J. Vac. Sci. Technol. A Vacuum, Surfaces, Film., **33**, 061506 (2015).

[4] E. Fortunato, P. Barquinha, A. Pimentel, L. Pereira, G. Goncalves, and R. Martins, Phys. Status Solidi - Rapid Res. Lett., **1**, p.34–36 (2007).

[5] N.L. Dehuff, E.S. Kettenring, D. Hong, H.Q. Chiang, J.F. Wager, R.L. Hoffman, C.H. Park, and D.A. Keszler, J. Appl. Phys. **97**, 064505 (2005).

[6] P. Barquinha, A. Pimentel, A. Marques, L. Pereira, R. Martins, and E. Fortunato, J. Non-Cryst. Solods **352**, p.1749 (2006).

[7] E.M.C. Fortunato, P.M.C. Barquinha, A.C.M.B.G. Pimentel, A.M.F. Gonçalves, A.J.S. Marques, L.M.N. Pereira, and R.F.P. Martins, Adv. Mater. **17**, 5, p.590-594 (2005).

[8] K. Kato, H. Matsui, H. Tabata, M. Takenaka, and S. Takagi, AIP Advances. **9**, 055001 (2019).

[9] K. Kato, H. Matsui, H. Tabata, M. Takenaka, and S. Takagi, IEEE Journal of the Electron Devices Society. **7**, p.1201-1208 (2019).

[10] I.X. Green, W. Tang, M. Neurock, and J.T. Yates. Jr, Science, **333**, 6043, p.736-739 (2011).

[11] Y.-R. Luo, *Comprehensive Handbook of Chemical Bond Energies* (CRC Press, New York, 2007), p. 667.

[12] Y.-R. Luo, *Comprehensive Handbook of Chemical Bond Energies* (CRC Press, New York, 2007), p. 1027.

[13] S. Aikawa, T. Nabatame, and K. Tsukagoshi, Appl. Phys. Lett., **103**, p.1–6 (2013).

[14] Q. Chen, B. Agrawal, and J. Meindl, IEEE Trans. Electron Devices. **49**, 6, p.1086–1090, (2002).

[15] A. M. Ionsescu and H. Riel, Nature. **479,** p.329-337 (2011).

[16] A.C. Seabaugh and Q. Zhang, IEEE. **98**, p.2095-2110 (2010).

[17] T.-J.K. Liu and K. Kuhn, *CMOS and Beyond* (Cambridge University Press), (2015).

[18] H. Lu and A.C. Seabaugh, IEEE J.Electron Devices Society, **2**, p.44-49 (2014).

[19] S. Takagi, M.-S. Kim, M. Noguchi, S.-M. Ji, K. Nishi, and M. Takenaka, Proc. VLSI Symp. p. T22-T23 (2015).

[20] S. Takagi, M. Noguchi, M. Kim, S.-H. Kim, C.-Y. Chang, M. Yokoyama, K. Nishi, R. Zhang, M. Ke, and M. Takenaka, Solid-State Electron. **125**, p.82-102 (2016).

[21] S. Takagi, D.H. Ahn, M. Noguchi, T. Gotow, K. Nishi, M. Kim, and M. Takenaka, IEDM Tech. Dig. p.516-519 (2016).

[22] H. Koinuma and I. Takeuchi, Nature Mat. **3**, p.429-438 (2004).

[23] K.S. Chang, M.L. Green, P.K. Schenck, I. Levin, and E. Venkatasubramanian, IEEE Transactions on Electron Devices. **59**, 12, p.3212-3216 (2012).

[24] R.J. Carter, E. Cartier, A. Kerber, L. Pantisano, T. Schram, S. De Gendt, and M. Heyns, Appl. Phys. Lett. **83**, p.533-535 (2003).

[25] Y. Mitani, H. Satake, and A. Toriumi, IEEE Transaction on Device and Materials Reliability. **8**, 1, p.6-13 (2008).

[26] D.A. Shirley, Phys. Rev. B. **5**, p.4709-4714 (1972).

[27] J. Musil, D. Heřman, and J. Šícha, J. Vac. Sci. Technol. A. **24**, 3, p.521-528 (2006)

[28] Y. Suzuki, T. Nagata, Y. Yamashita, T. Nabatame, A. Ogura and T. Chikyow, Jpn. J. Appl. Phys. **56**, 06GF11 (2017).

[29] T. Nagata, Y. Suzuki, Y. Yamashita, A. Ogura and T. Chikyow, Jpn. J. Appl. Phys. **57**, 04FJ04 (2018).

[30] S. M. Sze, Y. Li, and K.K. Ng, *Physics of Semiconductor Device* (Wiley, New York, 2021) 2nd ed. Part 3, Chapter 7, p.402.

Figure Captions

Fig. 1. Schematic illustration of (a) compositionally graded $Ti_xZn_{1-x}O_{1+x}$ film, $Ti_{0.3}Zn_{0.7}O_{1.3}$ films of (b) Single layer, (c) TiO_2 first, and (d) ZnO first sample structure.

Fig. 2. XRD patterns as a function of x value in $Ti_xZn_{1-x}O_{1+x}$. The inset shows 2D-XRD images near the (0002) reflection peak of ZnO with $x = 0$.

Fig. 3. RMS values and resistivities as a function of x value in $Ti_xZn_{1-x}O_{1+x}$. The insets show AFM images of ZnO and $Ti_{0.75}Zn_{0.25}O_{1.75}$.

Fig. 4. Area intensity ratio of Si-O to Si-Si bonding states of Si 2p spectra as a function of x value in $Ti_xZn_{1-x}O_{1+x}$ before and after post annealing. The inset shows the Si 2p spectrum of $Ti_{0.6}Zn_{0.4}O_{1.6}$.

Fig. 5. I-V characteristics for Single layer, TiO_2 first, and ZnO first

Fig. 6 Replots of I-V characteristics of (a) tunneling current and (b) Pool-Frenkel emission. The voltage range is 0.3 V to 1.0 V, respectively.

Fig. 7 AFM images of (a) Single layer, (b) TiO_2 first, and (c) ZnO first.

Fig. 8 (a) Zn $2p_{3/2}$, (b) Ti $2p_{3/2}$, and (c) O 1s spectra obtained by Al Kα-XPS.

Fig. 9. Si 1s spectra of Single layer, TiO_2 first and ZnO first normalized by Si bonding states obtained by Cr Kα-XPS. Solid circles and solid line correspond to the experimental data and fitted curve, respectively. Dashed lines represent the fitted curves for each bond: Si, SiO_2, $SiTiO_x$/$SiZnO_x$, and sub oxide (SiO_x).

Fig. 10. Experimental reflectivity and simulated curves of Single layer, TiO_2 first, and ZnO first measured by XRR. The fitting parameters of thickness and roughness of SiO_2 layers are indicated.

Fig. 11 The interfacial reactions of (a) Single layer, (b) TiO_2 first and (c) ZnO first.

Table 1 FWHM values and Ti composition ratio to Zn of Single layer, TiO_2 first and ZnO first calculated from the Zn 2p spectrum and Ti 2p spectrum.

Interface formation process	FWHM value calculated from Zn $2p_{3/2}$ spectrum	FWHM value calculated from Ti $2p_{3/2}$ spectrum	Ti composition ratio to Zn	$Zn2p_{3/2}$ peak position [eV]
Single layer	**1.62**	**1.27**	**0.70**	**1022.59**
TiO_2 first	**1.61**	**1.16**	**0.37**	**1022.44**
ZnO first	**1.62**	**1.15**	**0.35**	**1022.37**

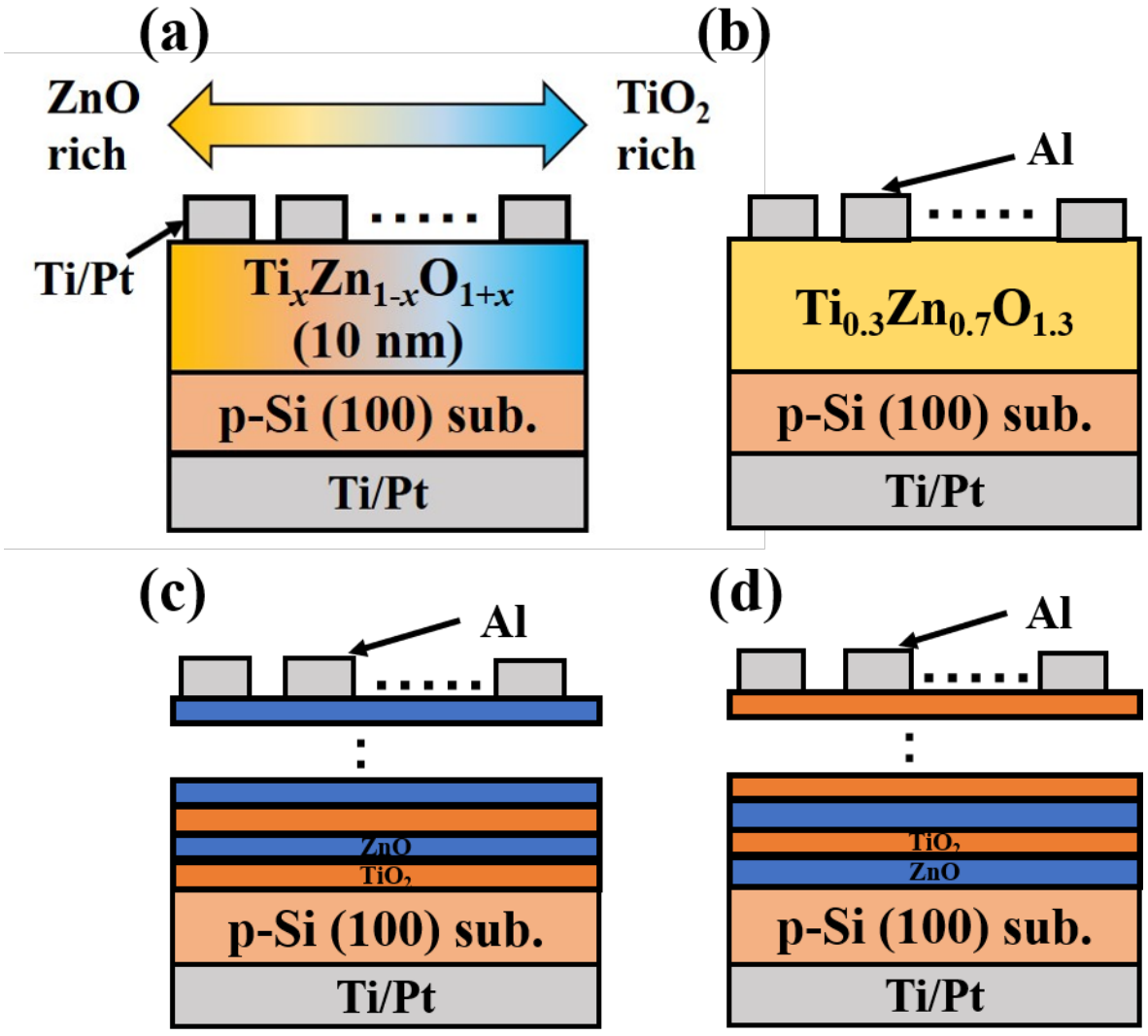
(a)
ZnO
rich
TiO2
rich
Ti/Pt
TixZn1-xO1+x
(10 nm)
p-Si (100) sub.
Ti/Pt
(b)
Al
Ti0.3Zn0.7O1.3
p-Si (100) sub.
Ti/Pt
(c)
Al
ZnO
TiO2
p-Si (100) sub.
Ti/Pt
(d)
Al
TiO2
ZnO
p-Si (100) sub.
Ti/Pt

Fig. 1.

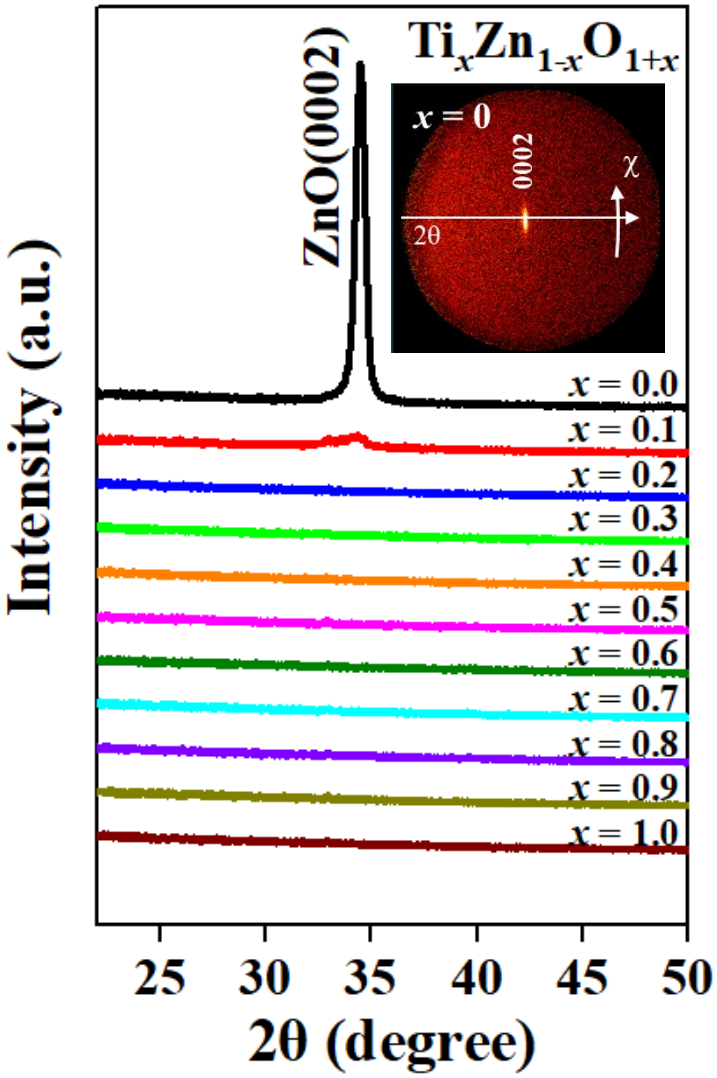
Ti$_x$Zn$_{1-x}$O$_{1+x}$
ZnO(0002)
x = 0
0002
χ
2θ
x = 0.0
x = 0.1
x = 0.2
x = 0.3
x = 0.4
x = 0.5
x = 0.6
x = 0.7
x = 0.8
x = 0.9
x = 1.0
Intensity (a.u.)
25
30
35
40
45
50
2θ (degree)

Fig. 2

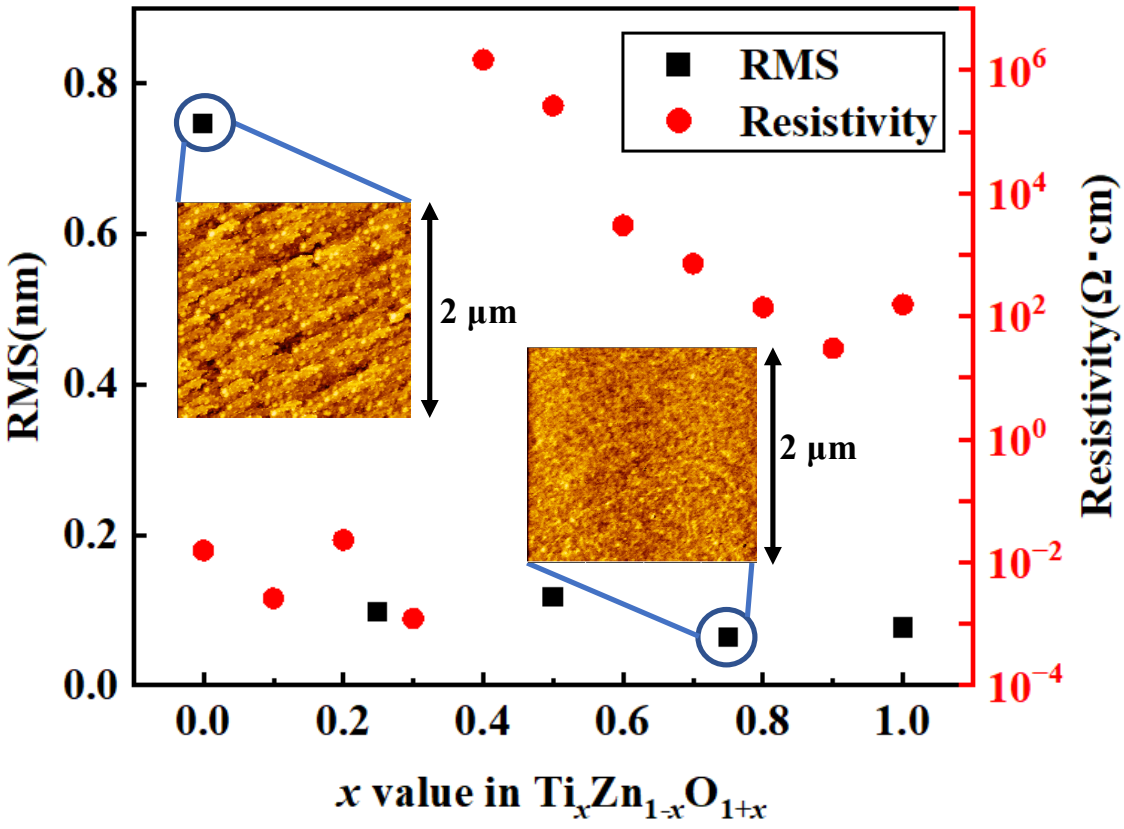
RMS
Resistivity
2 μm
2 μm
RMS(nm)
Resistivity(Ω·cm)
0.0
0.2
0.4
0.6
0.8
1.0
10^{6}
10^{4}
10^{2}
10^{0}
10^{-2}
10^{-4}
x value in $Ti_xZn_{1-x}O_{1+x}$

Fig. 3

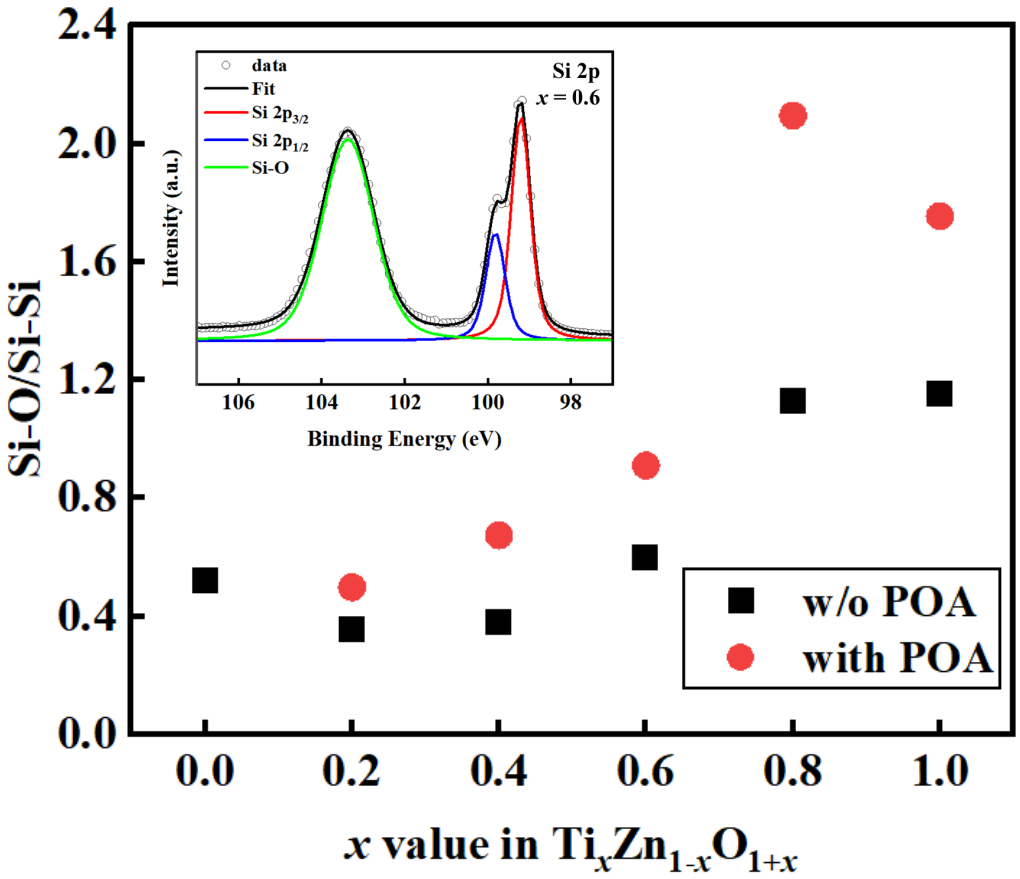
Si-O/Si-Si
2.4
2.0
1.6
1.2
0.8
0.4
0.0
0.0
0.2
0.4
0.6
0.8
1.0
x value in Ti$_x$Zn$_{1-x}$O$_{1+x}$
w/o POA
with POA
data
Fit
Si 2p$_{3/2}$
Si 2p$_{1/2}$
Si-O
Si 2p
x = 0.6
Intensity (a.u.)
106
104
102
100
98
Binding Energy (eV)

Fig. 4

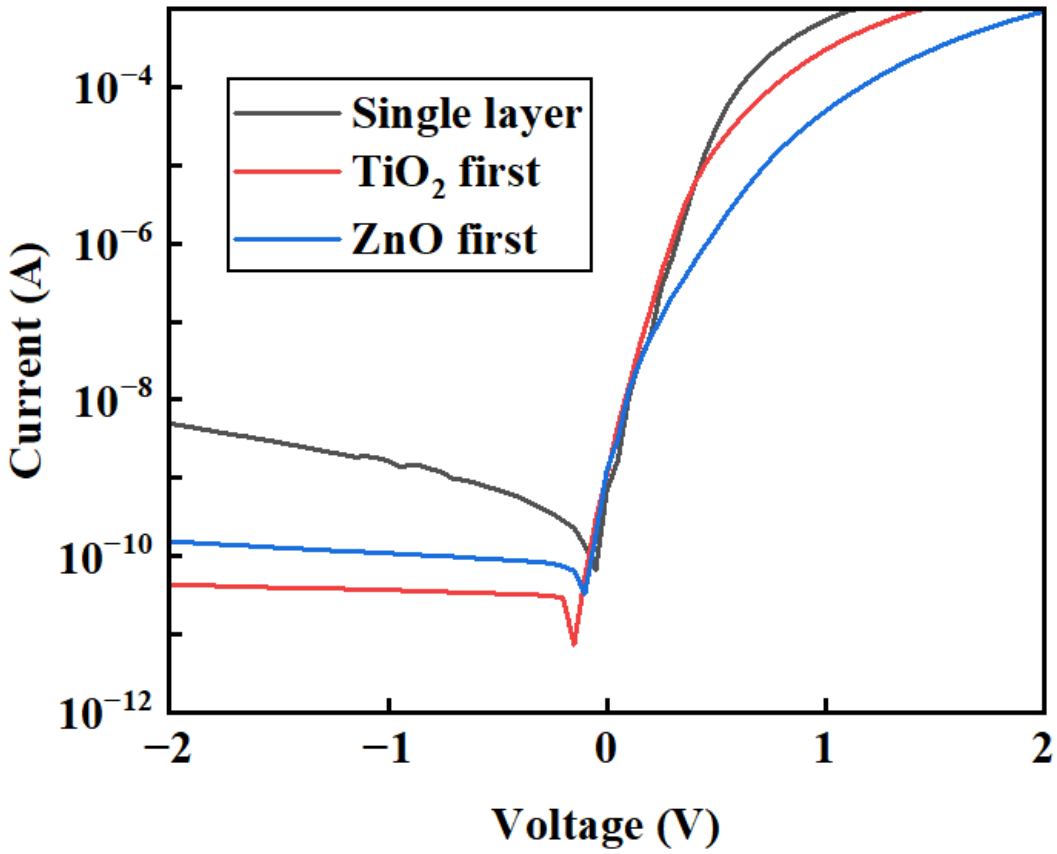
Single layer
TiO2 first
ZnO first
Current (A)
10−4
10−6
10−8
10−10
10−12
−2
−1
0
1
2
Voltage (V)

Fig. 5

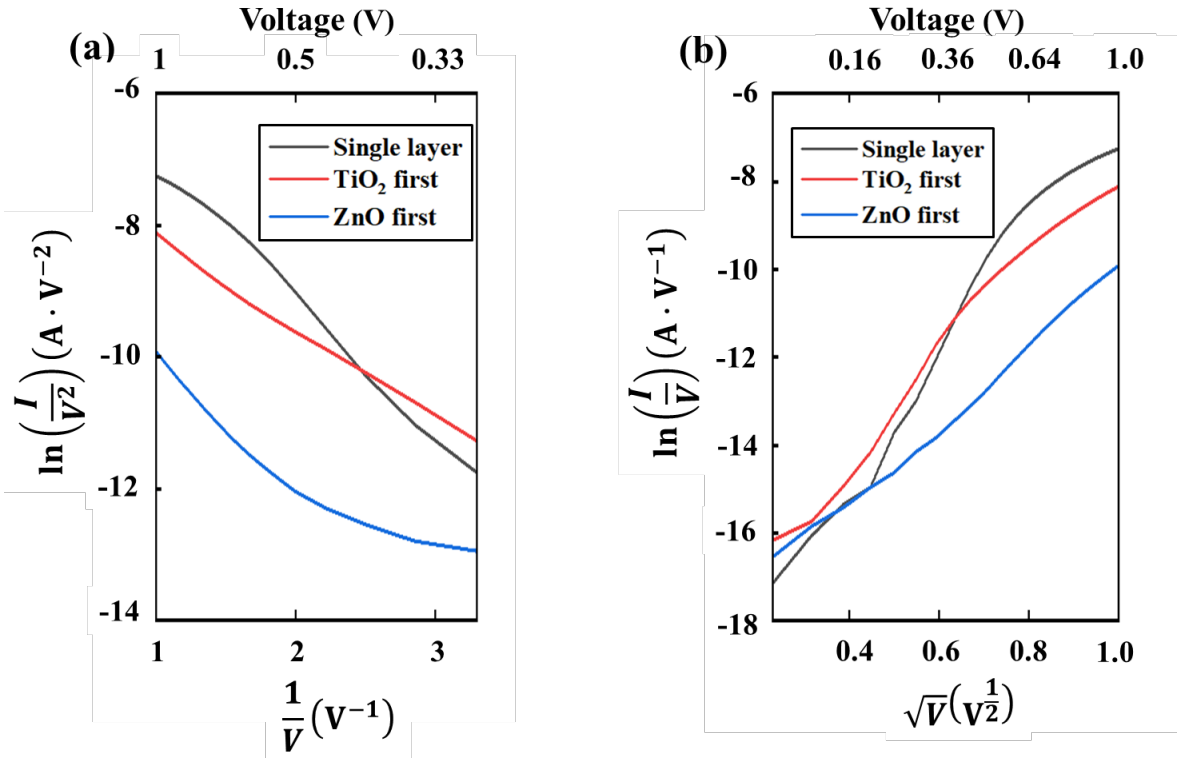
(a)
Voltage (V)
1
0.5
0.33
-6
-8
-10
-12
-14
Single layer
TiO2 first
ZnO first
1
2
3
ln(I/V²) (A·V⁻²)
1/V (V⁻¹)
(b)
Voltage (V)
0.16
0.36
0.64
1.0
-6
-8
-10
-12
-14
-16
-18
Single layer
TiO2 first
ZnO first
0.4
0.6
0.8
1.0
ln(I/V) (A·V⁻¹)
√V (V^1/2)

Fig. 6

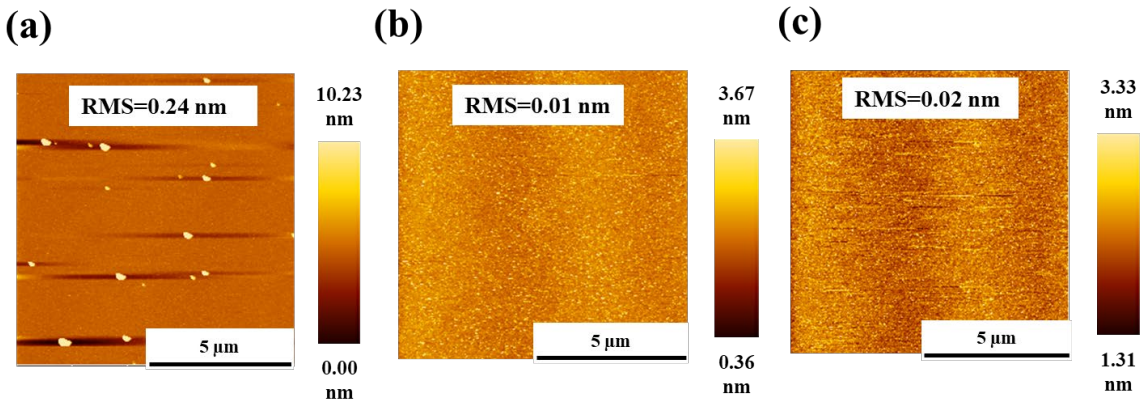
(a)
(b)
(c)
RMS=0.24 nm
10.23 nm
0.00 nm
5 µm
RMS=0.01 nm
3.67 nm
0.36 nm
5 µm
RMS=0.02 nm
3.33 nm
1.31 nm
5 µm

Fig. 7

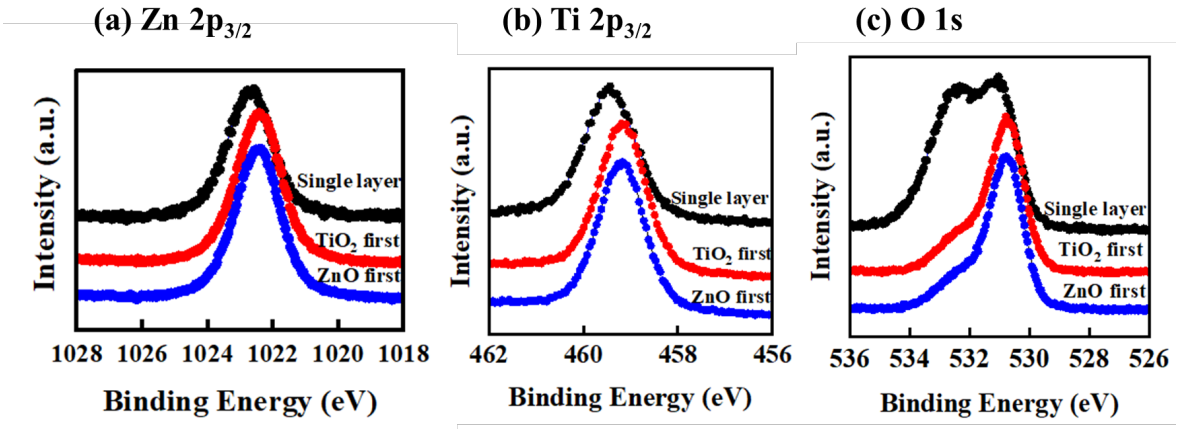
(a) Zn 2p3/2
(b) Ti 2p3/2
(c) O 1s
Intensity (a.u.)
Single layer
TiO2 first
ZnO first
1028 1026 1024 1022 1020 1018
462 460 458 456
536 534 532 530 528 526
Binding Energy (eV)

Fig. 8

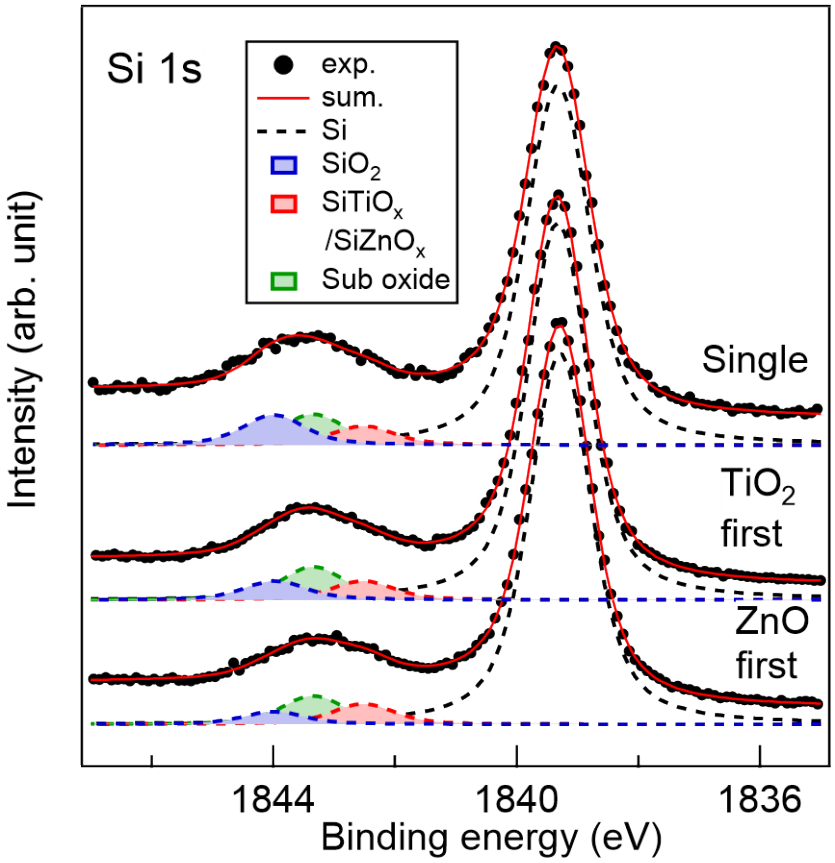
Si 1s
exp.
sum.
Si
SiO2
SiTiOx
/SiZnOx
Sub oxide
Single
TiO2
first
ZnO
first
Intensity (arb. unit)
1844
1840
1836
Binding energy (eV)

Fig. 9

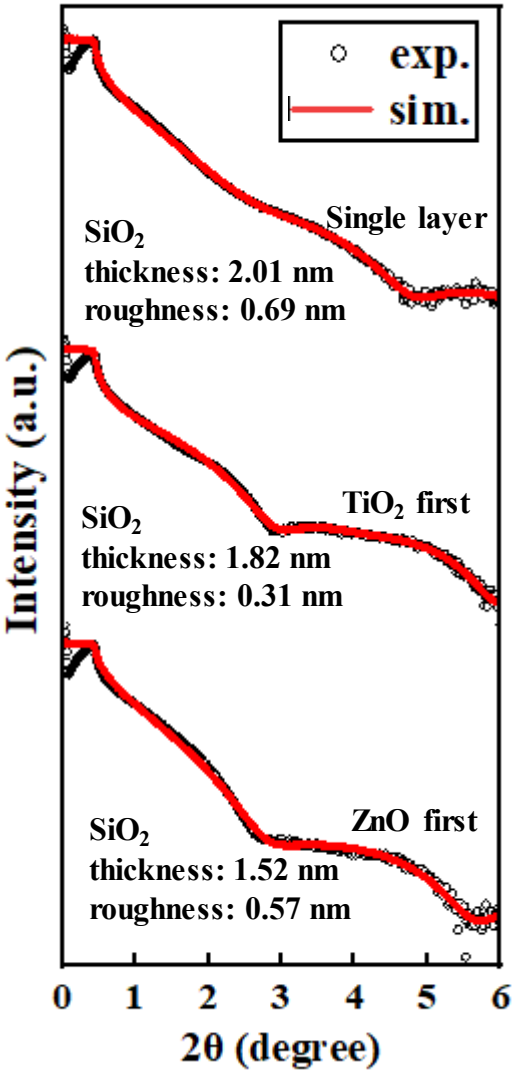
exp.
sim.
Single layer
SiO2
thickness: 2.01 nm
roughness: 0.69 nm
TiO2 first
SiO2
thickness: 1.82 nm
roughness: 0.31 nm
ZnO first
SiO2
thickness: 1.52 nm
roughness: 0.57 nm
Intensity (a.u.)
0
1
2
3
4
5
6
2θ (degree)

Fig. 10

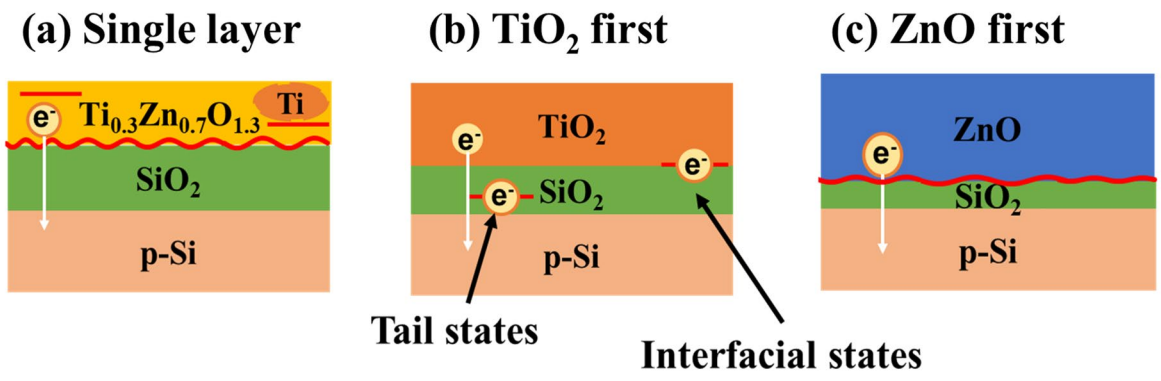
(a) Single layer
(b) TiO2 first
(c) ZnO first
e-
Ti0.3Zn0.7O1.3
Ti
SiO2
p-Si
TiO2
ZnO
Tail states
Interfacial states

Fig. 11